A novel size independent symplectic analytical singular element for inclined crack terminating at bimaterial interface

XF Hu[a, b], QS Shen[a, b], JN Wang[c], WA Yao[a, b*], ST Yang[d]

[a] *State Key Laboratory of Structural Analysis for Industrial Equipment, Dalian University of Technology, Dalian 116024, China*

[b] *International Research Center for Computational Mechanics*

[c] *Beijing Institute of Structure and Environment Engineering, Beijing, China*

[d] *Department of Civil and Environmental Engineering, the University of Strathclyde, Glasgow, G1 1XJ, United Kingdom*

[*] *Corresponding author: ywa@dlut.edu.cn*

Abstract: Cracks often exist in composite structures, especially at the interface of two different materials. These cracks can significantly affect the load bearing capacity of the structure and lead to premature failure of the structure. In this paper, a novel element for modeling the singular stress state around the inclined interface crack which terminates at the interface is developed. This new singular element is derived based on the explicit form of the high order eigen solution which is, for the first time, determined by using a symplectic approach. The developed singular element is then applied in finite element analysis and the stress intensity factors (SIFs) for a number of crack configurations are derived. It has been concluded that composites with complex geometric configurations of inclined interface cracks can be accurately simulated by the developed method, according to comparison of the results against benchmarks. It has been found that the stiffness matrix of the proposed singular element is independent on the element size and the SIFs of the crack can be solved directly without any post-processing.

Keywords: Composites, inclined interface crack, high order eigen solution, singular element, stress intensity factors

Nomenclature

$a^{(i)}, i = 1,2,3,...$	eigen expanding coefficients
$\boldsymbol{a}$	vector of the eigen expanding coefficients
A, B, C, D	coefficients of the general expression of eigenvector
$\boldsymbol{A}$	diagonal matrix of which the elements are composed of eigenvalues
$\boldsymbol{B}$	$\boldsymbol{B} = \boldsymbol{A}(\xi = \ln \rho)$
$\boldsymbol{C}$	matrix of the general expression of eigenvector
$\boldsymbol{d}$	vector of nodal displacements
$\boldsymbol{D}$	vector of the coefficients A, B, C, D
E, ν	Young's modulus and Poisson's ratio
$\boldsymbol{F}$	matrix generated from substituting eigenvector into the boundary condition
G	shearing modulus
$\boldsymbol{G}$	second part of the characteristic equation of eigenvector
$\boldsymbol{H}$	Hamiltonian operator matrix
$\boldsymbol{I}$	identity matrix
$\boldsymbol{J}$	unit symplectic matrix
$k_\alpha, k_\beta, k_\gamma, k_\eta$	$k = p, a, b, c, d$, coefficients in the relationship between the eigenvectors of the region #1 and the region #2
$k'_\alpha, k'_\beta, k'_\gamma, k'_\eta$	$k' = a', b', c', d'$, coefficients in the relationship between the eigenvectors of the region #3 and the region #2
K_I, K_{II}	mode I and mode II stress intensity factors
$\boldsymbol{K}$	stiffness matrix of the SASE
L	characteristic length
M , N	positive integers
$\boldsymbol{p}$, $\boldsymbol{q}$	vectors of the configuration variables and the dual variables
$\boldsymbol{p}^*$, $\boldsymbol{q}^*$	vectors of trail functions of the configuration variables and the dual variables
(r, θ)	polar coordinate system
$\boldsymbol{R}$	generalized stiffness matrix of the SASE
$S_r, S_\theta, S_{r\theta}$	generalized stress components
$S_r^*, S_\theta^*, S_{r\theta}^*$	trial functions of the generalized stress components
$\boldsymbol{T}_u$	matrix of which the elements are values of eigenvector on the export nodes
u_r, u_θ	displacement components
u_r^*, u_θ^*	trail functions of the displacement components
$\boldsymbol{Z}$	vector of the configuration variables and dual variables
$\boldsymbol{Z}^*$	vector of trail functions of the configuration variables and dual variables

α , β	the Dundurs parameters
ε	oscillation index (bimaterial constant)
$\varepsilon_r, \varepsilon_\theta, \varepsilon_{r\theta}$	strain components
$\sigma_r, \sigma_\theta, \sigma_{r\theta}$	stress components
ξ	generalized coordinate
$\theta_1, \theta_2, \theta_3, \theta_4$	$\theta_1 = -\pi - \omega$, $\theta_2 = -\pi$, $\theta_3 = 0$, $\theta_4 = \pi - \omega$
μ	eigenvalue
$\boldsymbol{\psi}$	eigenvector
$\psi_u, \psi_v, \psi_r, \psi_{r\theta}, \psi_\theta$	variables separated from displacement and stress variables
$\boldsymbol{\Phi}$, $\boldsymbol{\Theta}$	matrices of which the elements are composed of eigenvectors
$\boldsymbol{\Pi}$	deformation energy of the SASE
ρ	radius of the SASE
η	$\eta = E_2 / E_1$, the ratio of the Young's moduli of the two materials
ω	the angle represents crack orientation

1.Introduction

Composite materials are widely used in various engineering sectors due to their optimal properties compared with a single material. However, it is almost inevitable for the composite materials to possess cracks or defects, especially at the interfaces between two joining materials, under fabrication process, environmental degradation, applied loads, etc. The cracks can propagate, accumulate and significantly reduce the load bearing capacity of the structure in terms of fracture failure. Perhaps due to the mathematical complexities in formulating the interface crack, most of the existing studies in literature focused on a special case where the crack is along the interface of the two materials [1, 2, 3, 4, 5, 6, 7, 8, 9]. However, a more general and challenging case in which the crack lies in an angle with the interface and terminates at the interface should also be sufficiently addressed. Since the crack can be treated as being inclined from an interface crack, it is named inclined interface crack in this paper.

Stress Intensity Factors (SIFs) and Energy Release Rates (ERRs) have been widely employed for quantifying the stress singularity around the crack. Cook studied the stress state around the crack terminating at the bimaterial interface, and proposed a fracture criterion for crack initiation [10]. Lin and Mar considered the case in which the crack was perpendicular to the material interface. They developed a hybrid element to calculate the SIFs and the ERRs[11]. Chen derived a general expression for the singular stress field around the inclined interface crack, and employed the body force method to calculate the SIFs[12]. In addition, Wang and Per developed a model for solving the SIFs and the *T* stresses around the crack tip[13]. Lin and Sung[14] and Poonsawat *et al*.[15] analyzed the stress singularities of the inclined interface crack in anisotropic materials. Furthermore, Wijeyewickrema *et al*. studied the stress singularities of the crack terminating at the frictional interface of monoclinic bi-material composites[16].

Finite element (FE) analysis is popular in engineering applications; however, if conventional elements were used, extensive mesh refinement around the crack tip would have been employed to ensure the accuracy of simulation [17]. Different numerical methods have been developed to study crack problems in engineering including meshfree method [18, 19, 20, 21, 22], extended finite element method (XFEM) [23, 24, 25, 26, 27, 28], extended isogeometric analysis (XIA) [29, 30, 31]. These methods are used to calculate SIFs or ERRs for crack problems with high solving efficiency. However, only a few numerical methods can be applied to inclined crack terminating at bimaterial interface. Bouhala *et al*.[27] studied the inclined interface crack problem by using XFEM, the stress and displacement enrichment functions were determined by considering plane elasticity solution based on Airy functions. Natarajan *et al*. applied the extended scaled boundary finite element method (xSBFEM) to the inclined interface crack problem, and both SIFs and *T* stresses were solved numerically without path independent integral[32]. Nasri *et al*. investigated the behavior of the crack terminating at the zinc/steel bimaterial interface with different orientations by using the FE software package ABAQUS[33].

More recently, cohesive crack model is applied to the modeling of the bimaterial interface cracks. Adams modeled the crack which was perpendicular to the bimaterial interface and found that the critical value for crack propagation depended upon the maximum stress of the cohesive crack model, as well as the Dundures parameters[34]. Mehidi *et al*. investigated the crack normal to the metal/alumina interface by determining the *J* integral and the plastic zone at the crack tip using the three-dimensional finite element methods[35]. Muthu *et al*. developed a new variant of the element-free Galerkin (EFG) method, and applied this new method for the inclined bimaterial interface crack problem[36]. Chang and Jeng developed a "M_{int}" contour integral for the cracks passing through or terminating normally at the bimaterial interface[37].

For these existing methods in solving the inclined interface crack, the conventional FE analysis requires extensive mesh refinement around the crack tip and the solving efficiency is therefore reduced. XFEM[17] employs the asymptotic fields as the enrichment to improve the solving accuracy, however, it is still not satisfactory because, (1) dense meshes around the crack tip are also required to achieve acceptable accuracy; (2) the implementation in the XFEM is very complex. The elements isolated by the crack and the interface should be partitioned into subtriangles for the purpose of integration and the blending elements are required to connect the crack tip enriched element to the standard elements; (3) the numerical prediction is sensitive to the numerical integration scheme used for the enriched elements. In Ref.[27], different integration schemes were used for different types of elements, i.e., a thirteenth-order Gaussian integration method was used for the subtriangles at the crack tip, a sixth-order Gaussian integration scheme was used for the subtriangles at the crack surface and a sixteenth-order Gaussian integration scheme was used for the blending elements. In light of the existing methods in modeling the inclined interface cracks, it has been found that the description for the displacement and stress fields around the crack tip is of crucial importance. Although the enrichment terms as well as the standard FE shape functions are available in XFEM, further improvement is still desirable. Therefore, a combination of numerical method and analytical solution, which strictly satisfies all the fundamental equations, compatibility condition and the boundary condition, could bring many advantages. It is in this regard this paper is presented.

In this study, for the first time, the analytical eigen solution of the complex inclined interface crack is derived by using the symplectic method. Based on the obtained analytical eigen solution, a new symplectic analytical singular element (SASE) is developed for numerical simulation. The SIFs are then calculated directly without any post-processing. It should be noted that the stiffness matrix of the proposed SASE is proven independent on the element's size. This unique feature of the SASE plays an

important role in ensuring accuracy and stability of numerical simulation. The symplectic approach for elasticity[38, 39] has emerged as a useful tool for the analytical study of singularity problems. By using the symplectic approach, analytical eigen solutions for different crack problems were obtained[40, 41, 42, 43, 44, 45]. The rich information of displacement and stress fields around crack tip expressed in terms of analytical solution could lead to better solving accuracy and efficiency. Based on the existing analytical eigen solutions, a series of analytical singular elements were developed for the numerical study of cracks[46], bimaterial interface crack[40, 47], fatigue crack growth[48] and Dugdale model based cracks[49, 50]. These elements were termed as "singular element" or "enriched element" in the early publications [40, 46, 48, 49, 50]. However, considering the methodology used for construction of the element and its applications, the new developed elements in the recent publications [47, 51, 52, 53] were termed as Symplectic Analytical Singular Element (SASE). In the future, SASE will be consistently used.

A few examples are worked out to demonstrate the application of the proposed method. Verification of the results against the benchmarks has indicated that the developed model is very accurate in capturing the stress state around the inclined interface crack.

2.Fundamental equations

Considering an inclined interface crack terminating at the bimaterial interface as shown in Fig.1, the origin of the polar coordinate system is located at the crack tip. The crack orientation is denoted by $\theta = \pi - \omega$ where ω is an arbitrary angle satisfying $\pi \geq \omega \geq 0$. For a special case, the problem becomes a bimaterial interface crack problem[40] when $\omega = 0$ or $\omega = \pi$. The domain is divided into three regions by the crack and the material interface as shown in Fig.1. The subscript "i" ($i = 1,2,3$) is employed to represent each region. The Young's modulus and Poisson's ratio of the material in the ith region are E_i, ν_i. Since the regions #1 and #3 are occupied by the material 1 so we have $E_1 = E_3$ and $\nu_1 = \nu_3$. For the

sake of convenience, the subscript "i" ($i=1,2,3$) is omitted in the equations hereinafter except where it may cause confusion.

The fundamental equations of this problem under the assumption of plane stress are briefly presented below. The equilibrium equations neglecting the body force can be specified as follows,

$$\begin{cases} \dfrac{\partial \sigma_r}{\partial r}+\dfrac{\sigma_r-\sigma_\theta}{r}+\dfrac{1}{r}\dfrac{\partial \tau_{r\theta}}{\partial \theta}=0 \\ \dfrac{\partial \tau_{r\theta}}{\partial r}+\dfrac{2\tau_{r\theta}}{r}+\dfrac{1}{r}\dfrac{\partial \sigma_\theta}{\partial \theta}=0 \end{cases} \tag{1}$$

where σ_r, σ_θ and $\tau_{r\theta}$ are stress components. The relationship between strain and displacement is specified as follows

$$\begin{cases} \varepsilon_r=\dfrac{\partial u_r}{\partial r} \\ \varepsilon_\theta=\dfrac{u_r}{r}+\dfrac{1}{r}\dfrac{\partial u_\theta}{\partial \theta} \\ \gamma_{r\theta}=\dfrac{1}{r}\dfrac{\partial u_r}{\partial \theta}+\dfrac{\partial u_\theta}{\partial r}-\dfrac{u_\theta}{r} \end{cases} \tag{2}$$

where ε_r, ε_θ, $\gamma_{r\theta}$ are strain components, while u_r and u_θ are displacements along radial and angular directions respectively. The Hellinger-Reissner (**H-R**) variational principle of the discussed problem is specified by

$$\begin{aligned} \delta\sum_{i=1}^{3}\int_{\theta_i}^{\theta_{i+1}}\int_0^\infty \Bigg\{ & \sigma_{r,i}\frac{\partial u_{r,i}}{\partial r}+\frac{\sigma_{\theta,i}}{r}\left(\frac{\partial u_{\theta,i}}{\partial \theta}+u_{r,i}\right)+\tau_{r\theta,i}\left(\frac{\partial u_{\theta,i}}{\partial r}-\frac{u_{\theta,i}}{r}+\frac{1}{r}\frac{\partial u_{r,i}}{\partial \theta}\right) \\ & -\frac{1}{2E_i}\left[\sigma_{\theta,i}^2+\sigma_{r,i}^2-2\nu_i\sigma_{r,i}\sigma_{\theta,i}+2\left(1+\nu_i\right)\tau_{r\theta,i}^2\right]\Bigg\} r\mathrm{d}r\mathrm{d}\theta=0 \end{aligned} \tag{3}$$

where $\theta_1=-\pi-\omega$, $\theta_2=-\pi$, $\theta_3=0$ and $\theta_4=\pi-\omega$. Assuming that the two materials are perfectly bounded, then the compatibility condition at the material interface can be obtained by

$$u_{r,1}=u_{r,2},\quad u_{\theta,1}=u_{\theta,2},\quad \sigma_{\theta,1}=\sigma_{\theta,2},\quad \tau_{r\theta,1}=\tau_{r\theta,2},\quad \text{at } \theta=-\pi \tag{4}$$

$$u_{r,2}=u_{r,3},\quad u_{\theta,2}=u_{\theta,3},\quad \sigma_{\theta,2}=\sigma_{\theta,3},\quad \tau_{r\theta,2}=\tau_{r\theta,3},\quad \text{at } \theta=0 \tag{5}$$

The traction free boundary condition on the crack surfaces can be expressed as follows

$$\sigma_{\theta,1}=\tau_{r\theta,1}=0,\quad \text{at } \theta=-\pi-\omega \tag{6}$$

$$\sigma_{\theta,3}=\tau_{r\theta,3}=0,\quad \text{at } \theta=\pi-\omega \tag{7}$$

Due to the mathematical complexities, the problem described above is difficult to be solved by using conventional methods. This study employs a novel symplectic approach, by using which the original problem is transformed into a symplectic eigenvalue problem which is then solved analytically.

3.Symplectic approach

The symplectic approach for elasticity has been widely applied for the analytical study of singularity problems[38, 39]. By using this approach, the governing equation of the original problem is reduced into a series of first order differential equations which is then transformed into an eigenvalue problem by the method of separation of variables. The symplectic approach is employed in this study to solve the eigen solution of the complex inclined interface crack. By introducing the generalized coordinate

$$\xi=\ln r \tag{8}$$

and the generalized stress components

$$S_r=r\sigma_r,\quad S_\theta=r\sigma_\theta,\quad S_{r\theta}=r\tau_{r\theta} \tag{9}$$

the **H-R** variational principle expressed in Eq.(3) can be rewritten as

$$\begin{aligned}\delta\sum_{i=1}^{3}\int_{\theta_i}^{\theta_{i+1}}\int_0^{\infty}\Bigg\{&S_{r,i}\frac{\partial u_{r,i}}{\partial\xi}+S_{\theta,i}\left(\frac{\partial u_{\theta,i}}{\partial\theta}+u_{r,i}\right)+S_{r\theta,i}\left(\frac{\partial u_{\theta,i}}{\partial\xi}-u_{\theta,i}+\frac{1}{r}\frac{\partial u_{r,i}}{\partial\theta}\right)\\&-\frac{1}{2E_i}\left[S_{\theta,i}^2+S_{r,i}^2-2\nu_i S_{r,i}S_{\theta,i}+2\left(1+\nu_i\right)S_{r\theta,i}^2\right]\Bigg\}\mathrm{d}\xi\mathrm{d}\theta=0\end{aligned} \tag{10}$$

Making variation of Eq.(10) with respect to S_θ gives

$$S_\theta = E\left(u_r + \frac{\partial u_\theta}{\partial \theta}\right) + \nu S_r \tag{11}$$

Substituting Eq.(11) back into Eq.(10), the equivalent **H-R** variational principle can be further simplified as follows:

$$\begin{aligned}\delta\sum_{i=1}^{3}\int_{\theta_i}^{\theta_{i+1}}\int_0^\infty \Bigg\{ & S_{r,i}\frac{\partial u_{r,i}}{\partial \xi} + \nu_i S_{r,i}\left(u_{r,i} + \frac{\partial u_{\theta,i}}{\partial \theta}\right) + S_{r\theta,i}\left(\frac{\partial u_{\theta,i}}{\partial \xi} + \frac{\partial u_{r,i}}{\partial \theta} - u_{\theta,i}\right) \\ & \frac{E_i}{2}\left(u_{r,i} + \frac{\partial u_{\theta,i}}{\partial \theta}\right)^2 - \frac{1}{2E_i}\left[(1-\nu_i^2)S_{r,i}^2 + 2(1+\nu_i)S_{r\theta,i}^2\right]\Bigg\} \mathrm{d}\xi \mathrm{d}\theta = 0\end{aligned} \tag{12}$$

From Eq.(12), there are four independent variables in the equivalent **H-R** variational principle, i.e., u_r, u_θ, S_r and $S_{r\theta}$. Making variations of Eq.(12) with respective to these independent variables gives the symplectic dual equation which is specified by,

$$\frac{\partial \boldsymbol{Z}}{\partial \xi} = \boldsymbol{H}\boldsymbol{Z} \tag{13}$$

where $\boldsymbol{Z} = [u_r, u_\theta, S_r, S_{r\theta}]^{\mathrm{T}}$ is the unknown vector of the configuration variables $\boldsymbol{p} = [u_r, u_\theta]^{\mathrm{T}}$ and the dual variables $\boldsymbol{q} = [S_r, S_{r\theta}]^{\mathrm{T}}$. Moreover, the Hamiltonian operator matrix $\boldsymbol{H}$ is presented as follows,

$$\boldsymbol{H} = \begin{bmatrix} -\nu & -\nu\dfrac{\partial}{\partial\theta} & \dfrac{1-\nu^2}{E} & 0 \\ -\dfrac{\partial}{\partial\theta} & 1 & 0 & \dfrac{2(1+\nu)}{E} \\ E & E\dfrac{\partial}{\partial\theta} & \nu & -\dfrac{\partial}{\partial\theta} \\ -E\dfrac{\partial}{\partial\theta} & -E\dfrac{\partial^2}{\partial^2\theta} & -\nu\dfrac{\partial}{\partial\theta} & -1 \end{bmatrix} \tag{14}$$

The symplectic dual equation expressed in Eq.(13) can be solved by the method of separation of variables, let

$$\boldsymbol{Z}(\xi,\theta) = e^{\xi\mu}\boldsymbol{\psi}(\theta) \tag{15}$$

where μ is the symplectic eigenvalue and $\boldsymbol{\psi}(\theta)=[\psi_u \quad \psi_v \quad \psi_r \quad \psi_{r\theta}]^{\mathrm{T}}$ is the corresponding symplectic eigenvector. ψ_u, ψ_v, ψ_r and $\psi_{r\theta}$ are variables which are, respectively, separated from the original variables u_r, u_θ, S_r and $S_{r\theta}$. Similarly, ψ_θ is denoted as the variable separated from S_θ. Substituting Eq.(15) back into Eq.(13), the original problem is transformed into a symplectic eigenvalue problem, presented as follows,

$$\boldsymbol{H}\boldsymbol{\psi}(\theta)=\mu\boldsymbol{\psi}(\theta) \tag{16}$$

The eigenvalues of the Hamiltonian operator matrix $\boldsymbol{H}$ have some particular behavior that if a non-zero eigenvalue μ is an eigenvalue then $-\mu$ must also be an eigenvalue[38]. So the non-zero eigenvalues are divided into two groups,

(a) $\mu^{(\alpha,j)}, j=1,2,3,...,\mathrm{Re}(\mu^{(\alpha)})>0$ or, $\mathrm{Re}(\mu^{(\alpha)})=0$ and $\mathrm{Im}(\mu^{(\alpha)})>0$ (17)

(b) $\mu^{(\beta,j)}, j=1,2,3,...,\mu^{(\beta)}=-\mu^{(a)}$ (18)

The corresponding eigenvectors are denoted by $\boldsymbol{\psi}^{(\alpha,j)}$ and $\boldsymbol{\psi}^{(\beta,j)}$, respectively. The superscript $j=1,2,3,...$ is employed to denote the jth eigen solution, it will be ignored where applicable for the sake of simplicity. We define the symplectic inner product between two arbitrary vectors in the symplectic space as

$$<\boldsymbol{\psi}_a,\boldsymbol{\psi}_b>=\sum_{i=1}^{3}\int_{\theta_i}^{\theta_{i+1}}\boldsymbol{\psi}_a{}^{\mathrm{T}}\boldsymbol{J}\boldsymbol{\psi}_b\mathrm{d}\theta \tag{19}$$

where $\boldsymbol{J}=\begin{bmatrix}0 & \boldsymbol{I}\\ -\boldsymbol{I} & 0\end{bmatrix}$ is a unit symplectic matrix for the identity matrix $\boldsymbol{I}$ and the values of θ_1, θ_2, θ_3 and θ_4 have been defined above. It is proven that if μ is a single root, then the symplectic eigenvectors $\boldsymbol{\psi}^{(\alpha,j)}$ and $\boldsymbol{\psi}^{(\beta,j)}$ are mutually adjoint symplectic orthogonal to each other[38]. And if μ is a repeated root, the similar relationship also exists[38]. The mutually adjoint symplectic orthogonal relationship

among the eigenvectors are normally used to solve the exact solutions[43], it is introduced here just for completeness, more detailed discussions can be referred to Ref.[38].

By using the generalized stress components, the compatibility condition at the material interface expressed in Eqs.(4) and (5) can be rewritten as follows,

$$u_{r,1}=u_{r,2},\quad u_{\theta,1}=u_{\theta,2},\quad S_{\theta,1}=S_{\theta,2},\quad S_{r\theta,1}=S_{r\theta,2}\text{, at }\theta=-\pi \tag{20}$$

$$u_{r,2}=u_{r,3},\quad u_{\theta,2}=u_{\theta,3},\quad S_{\theta,2}=S_{\theta,3},\quad S_{r\theta,2}=S_{r\theta,3}\text{, at }\theta=0 \tag{21}$$

The traction free boundary condition on the crack surfaces can be rewritten as follows,

$$S_{\theta,1}=S_{r\theta,1}=0,\quad \text{at }\theta=-\pi-\omega \tag{22}$$

$$S_{\theta,3}=S_{r\theta,3}=0,\quad \text{at }\theta=\pi-\omega \tag{23}$$

4.Symplectic eigen solution

As formulated, the original problem has been transformed into a symplectic eigenvalue problem, e.g., in Eq.(16), subjected to compatibility condition and boundary condition. In solving the eigenvalue problem, the special case with zero eigenvalue and the general case with non-zero eigenvalue should be considered separately.

4.1.Zero eigenvalue and eigenvector

For zero eigenvalue, the corresponding eigenvector can be obtained by solving

$$\boldsymbol{H}\boldsymbol{\psi}(\theta)=0 \tag{24}$$

The eigenvectors can be obtained as follows,

$$\boldsymbol{\psi}^{(1)}=[\cos(\theta)\quad -\sin(\theta)\quad 0\quad 0]^{\mathrm{T}},\quad \boldsymbol{\psi}^{(2)}=[\sin(\theta)\quad \cos(\theta)\quad 0\quad 0]^{\mathrm{T}} \tag{25}$$

Obviously, they represent rigid body transitions along horizontal and vertical directions, respectively. Besides, it is found that the Jordan form eigenvectors exist and can be specified by

$$\boldsymbol{\psi}^{(1,J)} = \left[\frac{1-\nu}{2}\theta\sin(\theta) \quad \frac{1-\nu}{2}\theta\cos(\theta) - \frac{1+\nu}{2}\sin(\theta) \quad E\cos(\theta) \quad 0 \right]^{\mathrm{T}} \tag{26}$$

$$\boldsymbol{\psi}^{(2,J)} = \left[-\frac{1-\nu}{2}\theta\cos(\theta) \quad \frac{1-\nu}{2}\theta\sin(\theta) + \frac{1+\nu}{2}\cos(\theta) \quad E\sin(\theta) \quad 0 \right]^{\mathrm{T}} \tag{27}$$

where $\boldsymbol{\psi}^{(1,J)}$ and $\boldsymbol{\psi}^{(2,J)}$ are the Jordan form eigenvectors corresponding to $\boldsymbol{\psi}^{(1)}$ and $\boldsymbol{\psi}^{(2)}$, respectively. Combining the original eigenvectors and the corresponding Jordan form eigenvectors together, the Jordan form eigen solutions of the original problem can be determined and presented as follows

$$\boldsymbol{Z}^{(1,J)} = \boldsymbol{\psi}^{(1,J)} + \xi\boldsymbol{\psi}^{(1)}, \quad \boldsymbol{Z}^{(2,J)} = \boldsymbol{\psi}^{(2,J)} + \xi\boldsymbol{\psi}^{(2)} \tag{28}$$

It may be noted that the above Jordan form eigen solutions are concentrated forces acting at the coordinate origin along horizontal and vertical directions, respectively.

4.2.Non-zero eigenvalue and eigenvector

For non-zero eigenvalue, the general solution of the eigenvector of Eq.(16) for the material in the *i*th region can be solved and specified by

$$\boldsymbol{\psi}_i = \boldsymbol{C}_i\boldsymbol{D}_i, \quad (i = 1,2,3) \tag{29}$$

where the explicit expression of the matrix $\boldsymbol{C}_i$ is given in Eq.(A1) in the Appendix. $\boldsymbol{D}_i = [A_i \quad B_i \quad C_i \quad D_i]^{\mathrm{T}}$ is the vector of the coefficients A_i, B_i, C_i and D_i. There are totally 12 coefficients in the eigenvectors for the three regions whilst only four of them are independent. Therefore, only the coefficients of the region #2 (A_2, B_2, C_2 and D_2) are chosen as independent coefficients. The relationship among the coefficients is determined through the compatibility condition at the material interface as specified in Eqs.(20) and (21). Substituting the general solution of the eigenvector Eq.(29) into Eq.(20), the four coefficients of region #1 can be expressed by these of region #2, as specified by

$$\begin{cases} A_1 = a_\alpha p_\alpha A_2 + a_\beta p_\beta B_2 + a_\gamma p_\gamma C_2 + a_\eta p_\eta D_2 \\ B_1 = b_\alpha p_\alpha A_2 + b_\beta p_\beta B_2 + b_\gamma p_\gamma C_2 + b_\eta p_\eta D_2 \\ C_1 = c_\alpha p_\alpha A_2 + c_\beta p_\beta B_2 + c_\gamma p_\gamma C_2 + c_\eta p_\eta D_2 \\ D_1 = d_\alpha p_\alpha A_2 + d_\beta p_\beta B_2 + d_\gamma p_\gamma C_2 + d_\eta p_\eta D_2 \end{cases} \tag{30}$$

where the expressions of the coefficients k_α, k_β, k_γ, k_η ($k = p,a,b,c,d$) in the above equations are given in Eqs.(A3), (A4) and (A5) in the Appendix. Similarly, substituting Eq.(29) into Eq.(21) the coefficients of region #3 can also be represented by these of region #2, the relationship is specified by

$$\begin{cases} A_3 = a'_\alpha p_\alpha A_2 + a'_\gamma p_\gamma C_2 \\ B_3 = b'_\beta p_\beta B_2 + b'_\eta p_\eta D_2 \\ C_3 = c'_\alpha p_\alpha A_2 + c'_\gamma p_\gamma C_2 \\ D_3 = d'_\beta p_\beta B_2 + d'_\eta p_\eta D_2 \end{cases} \tag{31}$$

in which the expressions of the coefficients k'_α, k'_β, k'_γ, k'_η ($k' = a',b',c',d'$) are given in Eq.(A6) in the Appendix. In this way, the explicit forms of the eigenvectors $\boldsymbol{\psi}_1$, $\boldsymbol{\psi}_2$ and $\boldsymbol{\psi}_3$ for the three regions can be obtained with only four unknown coefficients A_2, B_2, C_2 and D_2. These coefficients can then be determined in accordance with the boundary condition on the crack surfaces.

Substituting the eigenvectors into the boundary condition expressed in Eqs.(22) and (23) leads to

$$\boldsymbol{F}(\mu)\boldsymbol{D}_2 = 0 \tag{32}$$

where the explicit expression of the matrix $\boldsymbol{F}(\mu)$ can be extracted from Eqs.(A7), (A8), (A9) and (A10) in the Appendix. If $\boldsymbol{D}_2$ has non-trivial solution, the determinant of the matrix $\boldsymbol{F}(\mu)$ must vanish, i.e.,

$$\det(\boldsymbol{F}(\mu)) = 0 \tag{33}$$

Expanding Eq.(33) leads to the characteristic equation of the eigenvalue as

$$\sin^2(\mu\pi)\boldsymbol{G}(\mu) = 0 \tag{34}$$

where

$$\begin{aligned}\boldsymbol{G}(\mu) = &[-\alpha+\beta^2+(1+\beta)(\alpha-\beta)(1-\cos 2\omega)\mu^2+(1-\beta^2)\cos(\mu\pi)\cos(\mu(\pi-2\omega))]^2 \\ &+(1-\beta^2)\sin^2(\mu(\pi-2\omega))[\beta^2-\alpha^2+(1-\beta^2)\cos^2(\mu\pi)]\end{aligned} \tag{35}$$

α and β are the Dundurs parameters as specified in Eq.(A2) in the Appendix.

The eigenvalue can be solved from Eq.(34) which is composed of two parts, solving the first part $\sin^2(\mu\pi)=0$ results in

$$\mu = \pm 1, \pm 2, \pm 3, \ldots \text{ (double root)} \tag{36}$$

In general, however, the second part of Eq.(34) is very complex and can only be solved numerically. Specially, for the bimaterial interface crack problem with $\omega = 0$ or $\omega = \pi$, the expression of $\boldsymbol{G}(\mu)$ is reduced into

$$\boldsymbol{G}(\mu) = \beta^2 \sin^2(\mu\pi) + \cos^2(\mu\pi) \tag{37}$$

For the crack perpendicular to the bimaterial interface ($\omega = \pi/2$ in this case), the expression of $\boldsymbol{G}(\mu)$ is reduced into

$$\boldsymbol{G}(\mu) = [-\alpha+\beta^2+2(1+\beta)(\alpha-\beta)\mu^2+(1-\beta^2)\cos(\mu\pi)]^2 \tag{38}$$

It is found that the obtained expressions of $\boldsymbol{G}(\mu)$ in Eqs.(37) and (38) are in line with the existing results[40], and this verifies the present model. As discussed, the second part of Eq.(34) is very complex and a numerical approach should be adopted to obtain the solution of the eigenvalue. Substituting the obtained eigenvalue back into Eq.(32), the non-trivial solution of $\boldsymbol{D}_2$ can be solved and then the eigenvectors for the three regions are all obtained through Eqs.(29), (30) and (31).

5.Stress intensity factors and T stress

The analytical solution of the inclined bimaterial interface crack problem can be expressed in the form of symplectic eigen expansion, specified as follows

$$\boldsymbol{Z} = \sum_{i=1}^{\infty} a^{(i)} e^{\xi \mu^{(i)}} \boldsymbol{\psi}^{(i)} \tag{39}$$

where $a^{(i)}$ is the unknown eigen expanding coefficient. Considering that the strain energy in the vicinity of the crack tip must be finite, hence the expanding terms involving the negative eigenvalue as given in Eq.(18) are not included in the above eigen expansion. Besides, the special case for concentrated forces acting on the crack tip is not considered in the present study, and hence the Jordan form eigen solutions which represent this special case are also neglected in Eq.(39).

In the eigen expansion, the first two terms are zero eigenvalue solutions (rigid body transitions), and the subsequent terms may bring stress singularity if any of the eigenvalue satisfies $1 > \mathrm{Re}(\mu^{(i)}) > 0$, ($i = 3,4,5,...$). The eigen expanding coefficients corresponding to these eigenvalues are of particular interest because they are the critical parameters which reflect the stress state around the crack tip. For most cases, it is found that $\mu^{(3)}$ and $\mu^{(4)}$ are the two eigenvalues which bring the stress singularity and they are also complex conjugates. The definition of the SIFs for inclined bimaterial interface crack in Ref.[17] is employed in this study, which can be specified as follows

$$\lim_{r\to 0}\left\{\sigma_\theta + \mathrm{i}\,\tau_{r\theta}\big|_{\theta=-\omega} = r^{\mathrm{Re}(\mu^{(3)})-1}\{(K_{\mathrm{I}} + \mathrm{i}K_{\mathrm{II}})\cos[\mathrm{Im}(\mu^{(3)})\ln(r/L)] + f(K_{\mathrm{I}}, K_{\mathrm{II}})\sin[\mathrm{Im}(\mu^{(3)})\ln(r/L)]\}\right\} \tag{40}$$

where $f(K_{\mathrm{I}}, K_{\mathrm{II}}) = -\mathrm{i}K_{\mathrm{I}} + K_{\mathrm{II}}$. It may be noted that the stress components in the vicinity of the crack tip ($r \to 0$ for this case) are dominated by the singularity terms in Eq.(39). Combining Eq.(39) and Eq.(40), the relationship between the SIFs and the expanding coefficients can be determined, as follows

$$K_{\mathrm{I}} = 2\sqrt{2\pi}\,\mathrm{Re}[a^{(3)}(L)^{-\mathrm{i}\cdot\mathrm{Im}(\mu^{(3)})}\psi_{\theta}^{(3)}(-\omega)], \quad K_{\mathrm{II}} = 2\sqrt{2\pi}\,\mathrm{Re}[a^{(3)}(L)^{-\mathrm{i}\cdot\mathrm{Im}(\mu^{(3)})}\psi_{r\theta}^{(3)}(-\omega)] \tag{41}$$

Specially, the eigenvalues of the case for bimaterial interface crack ($\omega = 0$ or $\omega = \pi$) can be determined analytically by solving Eq.(38) as follows,

$$\mu^{(3)}\left(,\mu^{(4)}\right) = \frac{1}{2} \pm \mathrm{i}\varepsilon, \quad \varepsilon = \frac{1}{2\pi}\ln\frac{1-\beta}{1+\beta} \tag{42}$$

The definition of the SIFs for this case is given by[40]

$$\lim_{r\to 0}\left\{\sigma_\theta+\mathrm{i}\,\tau_{r\theta}\big|_{\theta=0}=\frac{K_{\mathrm{I}}+\mathrm{i}K_{\mathrm{II}}}{\sqrt{2\pi r}}\left(\frac{r}{2L}\right)^{\mathrm{i}\varepsilon}\right\} \tag{43}$$

In addition, the relationship between the SIFs and the eigen expanding coefficients are

$$K_{\mathrm{I}}=2\sqrt{2\pi}\,\mathrm{Im}[a^{(3)}(2L)^{\mathrm{i}\varepsilon}\psi_{r\theta}(0)],\quad K_{\mathrm{II}}=2\sqrt{2\pi}\,\mathrm{Re}[a^{(3)}(2L)^{\mathrm{i}\varepsilon}\psi_{r\theta}(0)] \tag{44}$$

For the case where the crack is perpendicular to the bimaterial interface ($\omega=\pi/2$), it is proven that $\mu^{(3)}$ and $\mu^{(4)}$ are both real numbers. In this case, the definition of the SIFs[17] as well as the relationship between the SIFs and the eigen expanding coefficients can be specified by

$$\lim_{r\to 0}\left\{\sigma_\theta+\mathrm{i}\,\tau_{r\theta}\big|_{\theta=-\frac{\pi}{2}}=(K_{\mathrm{I}}+\mathrm{i}K_{\mathrm{II}})r^{\mu^{(3)}-1}\right\} \tag{45}$$

$$K_{\mathrm{I}}=a^{(3)}\psi_\theta^{(3)}(-\pi/2)+a^{(4)}\psi_\theta^{(4)}(-\pi/2),\quad K_{\mathrm{II}}=a^{(3)}\psi_{r\theta}^{(3)}(-\pi/2)+a^{(4)}\psi_{r\theta}^{(4)}(-\pi/2) \tag{46}$$

It should be pointed that the SIFs can be calculated directly without any post-processing once the eigen expanding coefficients are obtained.

Apart from the SIFs, the other higher order eigen expanding coefficients are also of importance in determining the stress field at a distance to the crack tip. For example, the expanding coefficients $a^{(5)}$ and $a^{(6)}$ actually form a constant stress field along the horizontal direction (also known as the T stress) since the corresponding eigenvalues are $\mu^{(5)}=\mu^{(6)}=1$ (double root). These expanding coefficients have been widely used in explaining physical phenomena[54], hence, determining these unknowns is necessary in analyzing the inclined crack problems. The proposed method can solve these unknowns directly without any post-processing, providing a deep insight into the stress field of the inclined interface crack. To the best of the authors' knowledge, there has not been a detailed study evaluating these higher order expanding coefficients.

6.Symplectic analytical singular element (SASE)

Conventional finite elements are usually not precise enough to represent the nature of the stress singularity around the crack tip. Moreover, the results are still unsatisfactory even though refined mesh around the crack tip is used. This is because the interior fields of conventional elements are defined by using regular polynomials which cannot represent the singular stress fields distributed around the crack tip properly. As stated in the previous sections, the exact solution of the stress and displacement is formed from the eigen solution through the symplectic eigen expansion defined in Eq.(39). Hence, the symplectic eigen solution is the best choice to represent the fields around the crack tip and as such the shortcomings for regular polynomials can be overcome naturally. Motivated by this, we propose the SASE as shown in Fig.2. Of this novel element, the interior fields are formed from the symplectic eigen solution obtained above. The area around the crack tip is occupied by the present circular SASE while the other area of the structure is meshed by using conventional elements. The radius of the SASE is denoted by ρ. The present SASE is connected with the surrounding conventional elements through the "export nodes" which are evenly distributed on the element's circumference. The node indexes are arranged from 1 to N, and the number of export nodes is not limited to a specific value, more export nodes will benefit the solution accuracy.

Assuming that the displacement and stress fields of the SASE are in the form of

$$\boldsymbol{Z}^* = [u_r^*, u_\theta^*, S_r^*, S_{r\theta}^*]^{\mathrm{T}} = \sum_{i=1}^{M} a^{(i)} e^{\xi \mu^{(i)}} \boldsymbol{\psi}^{(i)} \tag{47}$$

The variables u_r^*, u_θ^*, S_r^* and $S_{r\theta}^*$ in the above equation can be regarded as the trial functions of the displacements and generalized stresses, and the superscript "*" is used to differentiate from the exact solutions. Rewriting the trail functions in Eq.(47) in form of matrix gives

$$\boldsymbol{p}^* = [u_r^*, u_\theta^*]^{\mathrm{T}} = \boldsymbol{\Phi A a}, \quad \boldsymbol{q}^* = [S_r^*, S_{r\theta}^*]^{\mathrm{T}} = \boldsymbol{\Theta A a} \tag{48}$$

where $\boldsymbol{a}=[a^{(1)},a^{(2)},...a^{(M)}]^{\mathrm{T}}$ is the vector of the unknown expanding coefficients and the matrix $\boldsymbol{A}=diag(e^{\xi\mu^{(1)}},e^{\xi\mu^{(2)}},...,e^{\xi\mu^{(M)}})$ is the diagonal matrix of which the elements are composed of the eigenvalues. $\boldsymbol{p}^*$ and $\boldsymbol{q}^*$ are vectors of trail functions of the displacements and generalized stresses. The elements of the matrices $\boldsymbol{\Phi}$ and $\boldsymbol{\Theta}$ are extracted from the eigenvectors, and they are specified as follows

$$\boldsymbol{\Phi}=\begin{bmatrix}\psi_u^{(1)}(\theta),\psi_u^{(2)}(\theta),\psi_u^{(3)}(\theta),...\psi_u^{(M)}(\theta)\\ \psi_v^{(1)}(\theta),\psi_v^{(2)}(\theta),\psi_v^{(3)}(\theta),...\psi_v^{(M)}(\theta)\end{bmatrix} \tag{49}$$

$$\boldsymbol{\Theta}=\begin{bmatrix}\psi_r^{(1)}(\theta),\psi_r^{(2)}(\theta),\psi_r^{(3)}(\theta),...\psi_r^{(M)}(\theta)\\ \psi_{r\theta}^{(1)}(\theta),\psi_{r\theta}^{(2)}(\theta),\psi_{r\theta}^{(3)}(\theta),...\psi_{r\theta}^{(M)}(\theta)\end{bmatrix} \tag{50}$$

Substituting Eq.(48) back into the equivalent **H-R** variational principle Eq.(12) and considering that the trail functions have satisfied all the requirements of the fundamental equations and the boundary condition at the crack surfaces, the equivalent **H-R** variational principle can be furtherly simplified into

$$\delta\left[\sum_{j=1}^{3}\int_{\theta_j}^{\theta_{j+1}}\left[(\boldsymbol{p}_j^*)^{\mathrm{T}}\boldsymbol{q}_j^*\right]\Big|_{\xi=\ln\rho}\mathrm{d}\theta\right]=0 \tag{51}$$

The deformation energy $\boldsymbol{\Pi}$ of the SASE can be extracted from the above variational principle and specified by

$$\boldsymbol{\Pi}=\boldsymbol{a}^{\mathrm{T}}\boldsymbol{A}^{\mathrm{T}}\boldsymbol{R}\boldsymbol{A}\boldsymbol{a}\Big|_{\xi=\ln\rho} \tag{52}$$

where $\boldsymbol{R}$ is the generalized stiffness matrix of the SASE, as specified by

$$\boldsymbol{R}=\sum_{j=1}^{3}\int_{\theta_j}^{\theta_{j+1}}(\boldsymbol{\Phi}_j)^{\mathrm{T}}\boldsymbol{\Theta}_j\mathrm{d}\theta \tag{53}$$

In this way, the proposed SASE for modeling of the inclined bimaterial interface crack is constructed. However, from Eq.(52) it can be seen that the unknowns to be determined for the SASE in the current form are the eigen expanding coefficients. Because of the mismatch of the unknowns between the SASE

and conventional displacement elements, transition elements are required to connect the SASE to the conventional elements, and this will bring inconvenience in the implementation. In fact, this drawback can be overcome, and the details are introduced in the following section.

7.Discussions on the SASE

7.1.Displacement based form of the SASE

Denoting $\boldsymbol{d}=[u_r^{(1)},u_\theta^{(1)},...u_\theta^{(M)}]^{\mathrm{T}}$ as the vector of the nodal displacements where $u_r^{(j)}$ and $u_\theta^{(j)}$ ($j=1,2,...M$) are the displacement components of the jth export node of the SASE. It may be noted that the coordinates of the jth export node of the SASE under the polar coordinate system are (ρ,θ_j). Hence, the nodal displacement can easily be determined by substituting the coordinates (ρ,θ_j) into Eq.(48). Therefore, the following relationship can be obtained:

$$\boldsymbol{d}=[u_r^{(1)},u_\theta^{(1)},...u_\theta^{(M)}]^{\mathrm{T}}=\boldsymbol{T}_u\boldsymbol{B}\boldsymbol{a} \tag{54}$$

where $\boldsymbol{B}=\boldsymbol{A}(\xi=\ln\rho)$ and the elements of the matrix $\boldsymbol{T}_u$ are values of the eigenvector on the export nodes, specified as follows

$$\boldsymbol{T}_u=\begin{bmatrix}\psi_u^{(1)}(\theta_1) & \psi_u^{(2)}(\theta_1) & \psi_u^{(3)}(\theta_1) & ... & \psi_u^{(M)}(\theta_1)\\ \psi_v^{(1)}(\theta_1) & \psi_v^{(2)}(\theta_1) & \psi_v^{(3)}(\theta_1) & ... & \psi_v^{(M)}(\theta_1)\\ ... & & & & \\ \psi_v^{(1)}(\theta_N) & \psi_v^{(2)}(\theta_N) & \psi_v^{(3)}(\theta_N) & ... & \psi_v^{(M)}(\theta_N)\end{bmatrix} \tag{55}$$

From Eq.(54), the vector $\boldsymbol{a}$ can be expressed by $\boldsymbol{d}$ as

$$\boldsymbol{a}=\boldsymbol{B}^{-1}\boldsymbol{T}_u^{-1}\boldsymbol{d} \tag{56}$$

In the above equation, in order to get the inverse of the matrix $\boldsymbol{T}_u$ which is a M by $2N$ matrix, it is necessary to ensure that $\boldsymbol{T}_u$ is a square matrix, e.g. $M=2N$. For this purpose, once the number of the export nodes of the present SASE is chosen to be N, then the number of the expanding terms M in

Eq.(47) should be $2N$. Substituting Eq.(56) into Eq.(52) and noticing that $\boldsymbol{AB}^{-1} = \boldsymbol{I}$ when $\xi = \ln\rho$ gives

$$\boldsymbol{\Pi} = \boldsymbol{d}^{\mathrm{T}}\boldsymbol{T}_u^{-\mathrm{T}}\boldsymbol{R}\boldsymbol{T}_u^{-1}\boldsymbol{d} \tag{57}$$

Thus the stiffness matrix of the SASE can be specified by

$$\boldsymbol{K} = \boldsymbol{T}_u^{-\mathrm{T}}\boldsymbol{R}\boldsymbol{T}_u^{-1} \tag{58}$$

The nodal unknowns of the SASE are nodal displacements and hence it can be connected with conventional displacement elements directly without any transition element. Unlike the XFEM[3], the proposed SASE does not introduce any extra degree of freedoms (DOFs) on the export nodes.

7.2.Size independent stiffness matrix

There is infinite number of expanding terms in the analytical solution defined in Eq.(39), whilst in practice only a finite number can be selected in the trail function defined in Eq.(48). It is conceivable that choosing more terms will improve the representation of the trail function. However, the component $e^{\mu^{(i)}\ln\rho}$ contained in the higher order expanding terms could result in a huge number when the eigenvalue $\mu^{(j)}$ is very large. As a result, significant numerical error could be induced. Yet, in the proposed SASE such a risk is avoided naturally because $e^{\mu^{(i)}\ln\rho}$ is eliminated in the formulation of the stiffness matrix $\boldsymbol{K}$ defined in Eq.(58). Apparently, this novel property of SASE is beneficial to the stability and accuracy of the proposed method, especially when higher order eigen expanding terms are used.

Furthermore, it can be seen from Eq.(58) that the stiffness matrix of the SASE is independent on its radius ρ. In other words, the proposed SASE is a size independent element. It also means the stiffness matrices of different SASEs with different sizes are the same and they should not be calculated separately or repeatedly in the calculation. Instead, the stiffness matrix can be calculated in advance and

be used for all the SASEs with different sizes during the calculation. And this is particular efficient in the modeling which involves repeated calculations such as a parametric study on crack length. In those cases, the size of the SASE around the crack tip keeps changing during the updating of the mesh to match the changing crack length.

7.3.Integration of the stiffness matrix

From Eq.(53), it can be seen that the integration for the stiffness matrix of the SASE which is a two dimensional (2D) element is transformed into a one-dimensional (1D) integration. Besides, as all the components of the eigenvector are explicitly available, the integration in Eq.(53) can be done analytically without any difficulty. Because the SASE is a circular element so there exist overlapping areas with the connecting conventional elements, as shown in Fig.3. The contribution to the global stiffness matrix from the overlapping area is duplicated which leads to over estimation of the global stiffness matrix of the FE system and will introduce numerical error. Theoretically, the area of the overlapping region will be reduced to zero when infinite numbers of exporting nodes are used for the SASE. However, only finite numbers of export nodes can be used in practice and the overlapping area cannot be avoided. Nevertheless, in the previous studies for the crack problems it was proven that the resulted numerical error can be limited when sufficient numbers of the export nodes of the SASE are used [40, 46, 47]. It was shown that the numerical error of the predicted SIFs, with respect to the analytical solution, was -1.2% and -0.5% when 13 and 25 export nodes were used respectively [40]. Hence, in this study 25 export nodes are used to ensure the accuracy of the prediction.

7.4.Calculation of the SIFs and the solving procedures

By assembling the stiffness matrices of the SASEs and conventional elements into the global stiffness matrix, the original problem can be solved numerically. After solving the global equation, the nodal displacements of the SASEs can be obtained, and the SIFs can be calculated directly according to

Eqs.(56) and (41). Unlike other methods, the complex post-processing is unnecessary in the proposed method. The solving procedure is illustrated in Fig.4 for the convenience of readers.

7.5.Summary

In the above discussions, a SASE has been constructed for the modeling of the inclined bimaterial interface crack problem, and the new features of the proposed SASE include

- The SASE is a displacement based element which can be connected to the surrounding conventional elements directly without any transition element. Unlike the XFEM, the proposed SASE does not introduce any extra degree of freedoms (DOFs) on the export nodes.
- Unlike XFEM or other related methods, the interior fields of the present SASE are represented only by using the eigen solutions. And the stiffness matrix can be calculated analytically and the solving accuracy is therefore improved.
- The stiffness matrix is independent on the element size and this feature is beneficial to the numerical efficiency and stability.
- The SIFs can be calculated directly without any post-processing.

However, the crack and the material interface must be meshed explicitly in the model, and remeshing is requried if crack propagation problem is studied.

8.Numerical examples

Example 1: Considering an edge cracked bimaterial plate under tensile loading as shown in Fig.5, in which the FE mesh of the plate is also provided. The ratio of the Young's moduli of the two materials is denoted by $\eta = E_2 / E_1$. According to the previous study[40], a total of 25 export nodes of the SASE are used in all the numerical examples to ensure the solving accuracy. And it implies that the first 50 eigen expanding terms are selected in the construction of the SASE. The predictions on the non-dimensional

SIFs for different crack lengths are listed in Tab.1, and the numerical results of Ref.[1] obtained by using BEM are listed for comparison. It is found that the present results agree well with these of Ref.[1], and hence the present method is validated. Considering that the numerical results might be affected by the size of the SASE, we take the special case where $\eta = 2$ and $a/W = 0.1$ as an example to study the impact of the SASE's size ρ on the solving accuracy. The present predictions as well as the reference results[1] on K_I and K_{II} are shown in Fig.6, it is shown that the present predictions are stable and accuracy under a large range of the element size, and the reason for this satisfactory performance has been explained in the section 7.2. The contours of the stresses around the crack tip are shown in Fig.7, in which the stress concentration can be easily observed.

Example 2: Consider a square plate composed of two materials as shown in Fig.8, the geometric parameters are $W = 20$ and $a = 1$. The plate is subject to the tensile loading with $\sigma_1 = E_1$ and $\sigma_2 = E_2$. There are two crack tips in this model, and both of them are meshed using the present SASE. It may noted that the crack at the point B is a single material crack, and the formulation of the SASE for this problem has been reported in Ref.[46]. The present numerical predictions and the reference results of the non-dimensional SIFs $\sqrt{2}K_I/(\sigma_y a^{1-\mu_s})$ for the crack tip A and B are, respectively, listed in Tab.2 and Tab.3. For the crack tip A, the eigenvalue which brings the stress singularity is denoted by μ_s and also listed in Tab.2. Again, good agreements are found between the present predictions and the reference results from Refs[10, 11, 13].

Example 3: Consider the $4\text{mm} \times 4\text{mm}$ bimaterial square plate containing a crack terminating at the interface as shown in Fig.9, the material properties are $E_1 = 73\text{GPa}$, $\nu_1 = 0.17$, $E_2 = 206\text{GPa}$ and

$\nu_1 = 0.3$. The magnitude of the tensile loading is $\sigma_y = 1\text{MPa}$. By using the SASE around the crack tip, the SIFs are predicted for different crack orientations and the results are listed in Tab.4. The numerical results obtained by using extrapolation method on the FE results with extremely refined mesh reported in Ref.[17] are listed as a reference. According to the comparison, the present results agree very well with the reference results. Moreover, the computing cost of the present method is much more cheaper. In Ref.[17], the eight node plane element (quadratic element) is employed and a total of 382640 nodes are used in the mesh. But in the present study, the four node plane element (linear element) and a SASE are used and only 1425 nodes are used in the mesh.

Example 4: Considering the double edge cracked $80\text{mm} \times 80\text{mm}$ bimaterial plate as shown in Fig.10, the magnitude of the tensile loading is $\sigma_{yy} = 1\text{MPa}$. The ratio of the Young's moduli of the two materials is denoted by $\eta = E_2 / E_1$. The present predictions of the SIFs for different crack orientations are listed in Tab.5, Tab.6 and Tab.7. The numerical results of single material case obtained by using the quarter point singular element in the ANSYS software are also provided for comparison.

Example 5: Considering the structure as shown in Fig.11, the geometric parameters are given by $W = 20\text{mm}$ and $a = 6\text{mm}$, and the magnitude of the tensile loading is $\sigma_{yy} = 1\text{MPa}$. The Poisson's ratios of the two materials are $\nu_1 = \nu_2 = 0.2$. The ratio of the Young's moduli of the two materials is denoted by $\eta = E_2 / E_1$. Numerical results of the SIFs for crack the tip A and B are, respectively, listed in Tab.8 and Tab.9. Different crack orientations with $\omega = 30^\text{o}$, 45^o and 90^o are considered, and the values of crack orientation angle ω are specified in the brackets in the tables. It is interesting to find that with the increase of the Young's moduli ratio, the SIFs of the crack tip A increase while those of the crack tip B

decrease. This prediction implies that the inclined interface crack is attracted to propagate towards the stiffer material which is bounded to relatively softer material. And this trend is also affected by the inclined angle of the crack, e.g., the variation of the SIFs is significant when $\omega = 90^{o}$ but remains relatively small when $\omega = 30^{o}$. The numerical prediction could be used for the structure optimization of composite material for the case where the crack tends to propagate into the stiffer material, for example, to release certain healing agent embedded in the composite material. It should be noted that this is not within the scope of the present study and hence has not been addressed in this paper.

9.Conclusion

In this study, the inclined interface crack problem in composite has been investigated systematically from theoretical and computational aspects. By using the symplectic approach, the explicit forms of the eigen solution for the inclined interface crack were derived for the first time. The stress intensity factors (SIFs) for the cracks along, perpendicular to, and inclined to the interface were determined. Moreover, a new Symplectic Analytical Singular Element (SASE) has been developed based on the obtained symplectic eigen solution. It has been found that the composites with complex geometric configurations could be analyzed numerically by using the proposed SASE. In the worked examples, the first fifty symplectic eigen expanding terms were selected in the SASE to capture the stress state around the crack tip. Furthermore, the comparison between the present results and the benchmarks has indicated that the developed model is very accurate in capturing the stress state around the inclined interface crack.

10.Acknowledgements

The supports of the National Natural Science Foundation of China (No.11502045, and No. 11372065), the Fundamental Research Funds for the Central Universities (DUT15RC(3)029) are gratefully acknowledged.

11.Appendix

The expression of matrix $\boldsymbol{C}$ (in this case the subscript i is omitted for simplicity) in the general solution of the eigenvector is specified by

$$\boldsymbol{C}=\begin{bmatrix} \cos[(1+\mu)\theta] & \sin[(1+\mu)\theta] & \cos[(1-\mu)\theta] & \dfrac{3-\nu-\mu-\nu\mu}{3-\nu+\mu+\nu\mu}\sin[(1-\mu)\theta] \\ -\sin[(1+\mu)\theta] & \cos[(1+\mu)\theta] & -\dfrac{3-\nu+\mu+\nu\mu}{3-\nu-\mu-\nu\mu}\sin[(1-\mu)\theta] & \cos[(1-\mu)\theta] \\ \dfrac{E\mu}{1+\mu}\cos[(1+\mu)\theta] & \dfrac{E\mu}{1+\mu}\sin[(1+\mu)\theta] & \dfrac{E\mu(3-\mu)}{3-\nu-\mu-\nu\mu}\cos[(1-\mu)\theta] & \dfrac{E\mu(3-\mu)}{3-\nu+\mu+\nu\mu}\sin[(1-\mu)\theta] \\ \dfrac{E\mu}{1+\mu}\sin[(1+\mu)\theta] & \dfrac{E\mu}{1+\mu}\cos[(1+\mu)\theta] & \dfrac{E\mu(1-\mu)}{3-\nu-\mu-\nu\mu}\sin[(1-\mu)\theta] & -\dfrac{E\mu(1-\mu)}{3-\nu+\mu+\nu\mu}\cos[(1-\mu)\theta] \end{bmatrix} \tag{A1}$$

It is proven that the matrix $\boldsymbol{C}$ still remains unchanged when $\mu=1$.

In order to simplify the expressions, we define the parameters $\eta=E_2/E_1$ and $\gamma=(\nu_1-3)/(1+\nu_1)$ and introduce the Dundurs parameters[1]

$$\alpha=\frac{G_1(\kappa_2+1)-G_2(\kappa_1+1)}{G_1(\kappa_2+1)+G_2(\kappa_1+1)},\quad \beta=\frac{G_1(\kappa_2-1)-G_2(\kappa_1-1)}{G_1(\kappa_2+1)+G_2(\kappa_1+1)} \tag{A2}$$

The coefficients A_1, B_1, C_1 and D_1 in the eigenvector of region #1 can be expressed by those of region #2 with the following coefficients:

$$p_\alpha=\frac{(1+\nu_1)(1+\eta)}{2(1+\nu_2)},p_\beta=\frac{(1+\nu_1)(1+\eta)}{2(1+\nu_2)},p_\gamma=\frac{(1+\nu_1)(1+\eta)}{2(\mu+\nu_2+\mu\nu_2-3)},p_\eta=\frac{(1+\nu_1)(1+\eta)}{2(\mu-\nu_2+\mu\nu_2+3)} \tag{A3}$$

$$\begin{cases} a_\alpha=(1+\beta)-\mu(\alpha-\beta)\cos\left[2\pi(1+\mu)\right] \\ b_\alpha=\mu(\alpha-\beta)\sin\left[2\pi(1+\mu)\right] \\ c_\alpha=(\mu+\gamma)(\alpha-\beta)\cos(2\mu\pi) \\ d_\alpha=-(\mu-\gamma)(\alpha-\beta)\sin(2\mu\pi) \end{cases} \quad \begin{cases} a_\beta=\mu(\alpha-\beta)\sin\left[2\pi(1+\mu)\right] \\ b_\beta=(1+\beta)+\mu(\alpha-\beta)\cos\left[2\pi(1+\mu)\right] \\ c_\beta=-(\mu+\gamma)(\alpha-\beta)\sin(2\mu\pi) \\ d_\beta=(\gamma-\mu)(\alpha-\beta)\cos(2\mu\pi) \end{cases} \tag{A4}$$

$$\begin{cases} a_\gamma = \left[-\mu^2(\alpha-\beta)+(\alpha+\beta)\right]\cos(2\mu\pi)+2\mu\beta \\ b_\gamma = \left[\mu^2(\alpha-\beta)-(\alpha+\beta)\right]\sin(2\mu\pi) \\ c_\gamma = (\mu+\gamma)\left\{(1-\beta)+\mu(\alpha-\beta)\cos\left[2\pi(1-\mu)\right]\right\} \\ d_\gamma = \mu(\mu-\gamma)(\alpha-\beta)\sin\left[2\pi(1-\mu)\right] \end{cases} \quad \begin{cases} a_\eta = \left[\mu^2(\alpha-\beta)-(\alpha+\beta)\right]\sin(2\mu\pi) \\ b_\eta = \left[\mu^2(\alpha-\beta)-(\alpha+\beta)\right]\cos(2\mu\pi)+2\mu\beta \\ c_\eta = \mu(\mu+\gamma)(\alpha-\beta)\sin\left[2\pi(1-\mu)\right] \\ d_\eta = (-\mu+\gamma)\left\{(\beta-1)+\mu(\alpha-\beta)\cos\left[2\pi(1-\mu)\right]\right\} \end{cases} \tag{A5}$$

The coefficients A_3, B_3, C_3 and D_3 of the eigenvector of region #3 can be expressed by those of region #2 with the following coefficients:

$$\begin{cases} a'_\alpha = (1+\beta)-\mu(\alpha-\beta) \\ c'_\alpha = (\mu+\gamma)(\alpha-\beta) \\ b'_\beta = (1+\beta)+\mu(\alpha-\beta) \\ d'_\beta = (\gamma-\mu)(\alpha-\beta) \end{cases} \quad \begin{cases} a'_\gamma = \left[-\mu^2(\alpha-\beta)+(\alpha+\beta)\right]+2\mu\beta \\ c'_\gamma = (\mu+\gamma)\left[(1-\beta)+\mu(\alpha-\beta)\right] \\ b'_\eta = \left[\mu^2(\alpha-\beta)-(\alpha+\beta)\right]+2\mu\beta \\ d'_\eta = (-\mu+\gamma)\left[(\beta-1)+\mu(\alpha-\beta)\right] \end{cases} \tag{A6}$$

Substituting the eigenvectors into the boundary conditions Eq.(22) and (23) gives

$$\begin{aligned} &-\cos\left[(1+\mu)(\pi+\alpha)\right]\left(a_\alpha p_\alpha A_2 + a_\beta p_\beta B_2 + a_\gamma p_\gamma C_2 + a_\eta p_\eta D_2\right) \\ &+\sin\left[(1+\mu)(\pi+\alpha)\right]\left(b_\alpha p_\alpha A_2 + b_\beta p_\beta B_2 + b_\gamma p_\gamma C_2 + b_\eta p_\eta D_2\right) \\ &-\frac{1+\mu}{\gamma+\mu}\cos\left[(1-\mu)(\pi+\alpha)\right]\left(c_\alpha p_\alpha A_2 + c_\beta p_\beta B_2 + c_\gamma p_\gamma C_2 + c_\eta p_\eta D_2\right) \\ &+\frac{1+\mu}{\gamma-\mu}\sin\left[(1-\mu)(\pi+\alpha)\right]\left(d_\alpha p_\alpha A_2 + d_\beta p_\beta B_2 + d_\gamma p_\gamma C_2 + d_\eta p_\eta D_2\right) = 0 \end{aligned} \tag{A7}$$

$$\begin{aligned} &\sin\left[(1+\mu)(\pi+\alpha)\right]\left(a_\alpha p_\alpha A_2 + a_\beta p_\beta B_2 + a_\gamma p_\gamma C_2 + a_\eta p_\eta D_2\right) \\ &+\cos\left[(1+\mu)(\pi+\alpha)\right]\left(b_\alpha p_\alpha A_2 + b_\beta p_\beta B_2 + b_\gamma p_\gamma C_2 + b_\eta p_\eta D_2\right) \\ &+\frac{1-\mu}{\gamma+\mu}\sin\left[(1-\mu)(\pi+\alpha)\right]\left(c_\alpha p_\alpha A_2 + c_\beta p_\beta B_2 + c_\gamma p_\gamma C_2 + c_\eta p_\eta D_2\right) \\ &+\frac{1-\mu}{\gamma-\mu}\cos\left[(1-\mu)(\pi+\alpha)\right]\left(d_\alpha p_\alpha A_2 + d_\beta p_\beta B_2 + d_\gamma p_\gamma C_2 + d_\eta p_\eta D_2\right) = 0 \end{aligned} \tag{A8}$$

$$\begin{aligned} &-\cos\left[(1+\mu)(\pi-\alpha)\right]\left(a'_\alpha p_\alpha A_2 + a'_\gamma p_\gamma C_2\right) - \sin\left[(1+\mu)(\pi-\alpha)\right]\left(b'_\beta p_\beta B_2 + b'_\eta p_\eta D_2\right) \\ &-\frac{1+\mu}{\gamma+\mu}\cos\left[(1-\mu)(\pi-\alpha)\right]\left(c'_\alpha p_\alpha A_2 + c'_\gamma p_\gamma C_2\right) - \frac{1+\mu}{\gamma-\mu}\sin\left[(1-\mu)(\pi-\alpha)\right]\left(d'_\beta p_\beta B_2 + d'_\eta p_\eta D_2\right) = 0 \end{aligned} \tag{A9}$$

$$-\sin\left[(1+\mu)(\pi-\alpha)\right]\left(a'_{\alpha}p_{\alpha}A_2+a'_{\gamma}p_{\gamma}C_2\right)+\cos\left[(1+\mu)(\pi-\alpha)\right]\left(b'_{\beta}p_{\beta}B_2+b'_{\eta}p_{\gamma}D_2\right)$$
$$-\frac{1-\mu}{\gamma+\mu}\sin\left[(1-\mu)(\pi-\alpha)\right]\left(c'_{\alpha}p_{\alpha}A_2+c'_{\gamma}p_{\gamma}C_2\right)+\frac{1-\mu}{\gamma-\mu}\cos\left[(1-\mu)(\pi-\alpha)\right]\left(d'_{\beta}p_{\beta}B_2+d'_{\eta}p_{\gamma}D_2\right)=0 \tag{A10}$$

Obviously, the components of the matrix $\boldsymbol{F}(\mu)$ in Eq.(32) can be extracted from Eqs.(A7), (A8), (A9) and (A10) without any difficulty. However, considering that the expression of the matrix $\boldsymbol{F}(\mu)$ is very large, it is left to the readers.

12.References

[1]. Miyazaki N, Ikeda T, Soda T, Munakata T. Stress intensity factor analysis of interface crack using boundary element method-application of contour-integral method. Engineering Fracture Mechanics, 1993, 45:599-610.

[2]. Bjerkén C, Persson C. A numerical method for calculating stress intensity factors for interface cracks in bimaterials. Engineering Fracture Mechanics, 2001, 68: 235-246.

[3]. Liu XY, Xiao QZ, Karihaloo BL. XFEM for direct evaluation of mixed mode SIFs in homogeneous and bi-materials. International Journal for Numerical Methods in Engineering, 2004, 59: 1103-1118.

[4]. Hemanth D, Aradhya KSS, Murthy TSR, Govinda Raju N. Strain energy release rates for an interface crack in orthotropic media--a finite element investigation. Engineering Fracture Mechanics, 2005, 72: 759-772.

[5]. Agrawal A, Karlsson AM. Obtaining mode mixity for a bimaterial interface crack using the virtual crack closure technique. International Journal of Fracture, 2006, 141: 75-98.

[6]. Sharma K, Bui TQ, Zhang CZ, Bhargava RR. Analysis of a subinterface crack in piezoelectric bimaterials with the extended finite element method. Engineering Fracture Mechanics, 2013, 104: 114-139.

[7]. Menk A, Bordas S. Numerically determined enrichment functions for the extended finite element method and applications to bi-material anisotropic fracture and polycrystals. International Journal for Numerical Methods in Engineering, 2010, 83: 805-828.

[8]. Ma P, Su RKL, Feng WJ. Fracture analysis of an electrically conductive interface crack with a contact zone in a magnetoelectroelastic bimaterial system. International Journal of Solids and Structures, 2015, 53: 48-57.

[9]. Banks-Sills L, Farkash E. A note on the Virtual Crack Closure Technique for a bimaterial interface crack. International Journal of Fracture, 2016: 1-10.

[10]. Cook TS, Erdogan F. Stresses in bonded materials with a crack perpendicular to the interface. International Journal of Engineering Science, 1972, 10:677-697.

[11]. Lin KY, Mar JW. Finite element analysis of a stress intensity factors for crack at a bimaterial interface. International Journal of Fracture, 1976, 12:521-531.

[12]. Chen DH. A crack normal to and terminating at a bimaterial interface. Engineering Fracture Mechanics, 1994, 49:517-523.
[13]. Wang TZ, Per S. A crack perpendicular to and terminating at a bimaterial interface. Acta Mechanica Sinica, 1998, 14(1):27-36.
[14]. Lin YY, Sung JC. Singularities of an inclined crack terminating at an anisotropic bimaterial interface. International Journal of Solids and Structures, 1997, 34: 3727-3754.
[15]. Poonsawat P, Wijeyewickrema AC, Karasudhi P. Stress singularity analysis of a crack terminating at the interface of an anisotropic layered composite. Journal of Applied Mechanics, 1998, 65: 829-836.
[16]. Wijeyewickrema AC, Poonsawat P, Karasudhi P. Stress singularities of a crack terminating at the frictional interface of a monoclinic bimaterial composite. Materials Science and Engineering: A, 2000, 285: 397-407.
[17]. Chang J, Xu JQ. The singular stress field and stress intensity factors of a crack terminating at a bimaterial interface. International Journal of Mechanical Sciences, 2007, 49: 888-897.
[18]. Tanaka S, Suzuki H, Sadamoto S, Okazawa S, Yu TT, Bui TQ. Accurate evaluation of mixed-mode intensity factors of cracked shear-deformable plates by an enriched meshfree Galerkin formulation. Archive of Applied Mechanics, 2016: 1-20.
[19]. Khosravifard A, Hematiyan M R, Bui T Q, Do TV. Accurate and efficient analysis of stationary and propagating crack problems by meshless methods. Theoretical and Applied Fracture Mechanics, 2017, 87: 21-34.
[20]. Tanaka S, Suzuki H, Sadamoto S, Sannomaru S, Yu TT, Bui TQ. J-integral evaluation for 2D mixed-mode crack problems employing a meshfree stabilized conforming nodal integration method. Computational Mechanics, 2016, 58(2): 185-198.
[21]. Tanaka S, Suzuki H, Sadamoto S, Imachi M, Bui TQ. Analysis of cracked shear deformable plates by an effective meshfree plate formulation. Engineering Fracture Mechanics, 2015, 144: 142-157.
[22]. Nguyen NT, Bui TQ, Zhang CZ, Truong TT. Crack growth modeling in elastic solids by the extended meshfree Galerkin radial point interpolation method. Engineering Analysis with Boundary Elements, 2014, 44: 87-97.
[23]. Kang ZY, Bui TQ, Nguyen DD, Saitoh T, Hirose S. An extended consecutive-interpolation quadrilateral element (XCQ4) applied to linear elastic fracture mechanics. Acta Mechanica, 2015, 226: 3991-4015.
[24]. Zhang X, Bui TQ. A fictitious crack XFEM with two new solution algorithms for cohesive crack growth modeling in concrete structures. Engineering Computations, 2015, 32: 473-497.
[25]. Kang Z, Bui TQ, Saitoh T, Hirose S. Quasi-static crack propagation simulation by an enhanced nodal gradient finite element with different enrichments. Theoretical and Applied Fracture Mechanics, 2017, 87: 61-77.
[26]. Yu T, Bui TQ, Liu P, Zhang CZ, Hirose S. Interfacial dynamic impermeable cracks analysis in dissimilar piezoelectric materials under coupled electromechanical loading with the extended finite element method. International Journal of Solids and Structures, 2015, 67: 205-218.
[27]. Bouhala L, Shao Q, Koutsawa Y, Younes A, Nunez P, Makradi A, Belouettar S. An XFEM crack-tip enrichment for a crack terminating at a bi-material interface. Engineering Fracture Mechanics, 2013, 102: 51-64.
[28]. Bhattacharya S, Singh IV, Mishra BK, Bui TQ. Fatigue crack growth simulations of interfacial cracks in bi-layered FGMs using XFEM. Computational Mechanics, 2013, 52: 799-814.

[29]. Bui TQ. Extended isogeometric dynamic and static fracture analysis for cracks in piezoelectric materials using NURBS. Computer Methods in Applied Mechanics and Engineering, 2015, 295: 470-509.
[30]. Bui TQ, Hirose S, Zhang CZ, Rabczuk T, Wu CT, Saitoh T, Lei J. Extended isogeometric analysis for dynamic fracture in multiphase piezoelectric/piezomagnetic composites. Mechanics of Materials, 2016, 97: 135-163.
[31]. Singh SK, Singh IV, Mishra BK, Bhardwaj G, Bui TQ. A simple, efficient and accurate Bézier extraction based T-spline XIGA for crack simulations. Theoretical and Applied Fracture Mechanics, 2017, 88: 74-96.
[32]. Natarajan S, Song CM, Belouettar S. Numerical evaluation of stress intensity factors and T-stress for interfacial cracks and cracks terminating at the interface without asymptotic enrichment. Computer Methods in Applied Mechanics and Engineering, 2014, 279: 86-112.
[33]. Nasri K, Abbadi M, Zenasni M, Azari Z. Numerical and experimental study of crack behaviour at the zinc/TRIP steel 800 interface. Computational Materials Science, 2014, 82: 172-177.
[34]. Adams GG. Critical value of the generalized stress intensity factor for a crack perpendicular to an interface. Proc. R. Soc. A. The Royal Society, 2015, 471: 20150571.
[35]. Mehidi A, Kaddouri K, Belhouari M, Amiri A, Bachir Bouiadjra B. Three-dimensional finite element analysis of a crack normal to and terminating at a bi-material interface. Journal of the Brazilian Society of Mechanical Sciences and Engineering, 2015, 37: 1785-1792.
[36]. Muthu N, Maiti S K, Falzon BG, Yan W. Crack propagation in non-homogenous materials: Evaluation of mixed-mode SIFs, T-stress and kinking angle using a variant of EFG Method. Engineering Analysis with Boundary Elements, 2016, 72: 11-26.
[37]. Chang JH, Jeng BS. M- and M_{int}-integrals for cracks normal to the interface of anisotropic bimaterials. International Journal of Fracture, 2016, 197: 49-61.
[38]. Yao WA, Zhong WX, Lim CW. Symplectic Elasticity. Singapore, World scientific, 2009.
[39]. Lim CW, Xu XS. Symplectic elasticity: theory and applications. Applied Mechanics Reviews, 2010, 63: 050802.
[40]. Hu XF, Yao WA. A novel singular finite element on mixed-mode bimaterial interfacial cracks with arbitrary crack surface tractions. International Journal of Fracture, 2011, 172: 41-52.
[41]. Wang JS, Qin QH. Symplectic model for piezoelectric wedges and its application in analysis of electroelastic singularities. Philosophical Magazine, 2007, 87: 225-251.
[42]. Xu CH, Zhou ZH, Xu XS, Leung AYT. Electroelastic singularities and intensity factors for an interface crack in piezoelectric–elastic bimaterials. Applied Mathematical Modelling, 2015, 39: 2721-2739.
[43]. Zhou ZH, Xu XS, Leung AYT. Mode III edge-crack in magneto-electro-elastic media by symplectic expansion. Engineering Fracture Mechanics, 2010, 77: 3157-3173.
[44]. Zhou ZH, Xu XS, Leung AYT. Hamiltonian analysis of a magnetoelectroelastic notch in a mode III singularity. Smart Materials and Structures, 2013, 22: 095018.
[45]. Zhang HW, Zhong WX. Hamiltonian principle based stress singularity analysis near crack corners of multi-material junctions. International Journal of Solids and Structures, 2003, 40: 493-510.
[46]. Yao WA, Hu XF. A novel singular finite element of mixed-mode crack problems with arbitrary crack tractions. Mechanics Research Communications, 2011, 38: 170-175.
[47]. Hu XF, Wang JN, Yao WA. A size independent enriched finite element for the modeling of bimaterial interface cracks. Computers & Structures, 2016, 172: 1-10.

[48]. Hu XF, Yao WA. A new enriched finite element for fatigue crack growth. International Journal of Fatigue, 2013, 48: 247-256.
[49]. Yao WA, Hu XF. A Novel Singular Finite Element on Mixed-Mode Dugdale Model Based Crack. Journal of Engineering Materials and Technology, 2012, 134: 021003.
[50]. Yao WA, Hu XF. A singular finite element on the mixed-mode bimaterial interfacial cracks. International Journal for Computational Methods in Engineering Science and Mechanics, 2012, 13: 219-226.
[51]. Hu XF, Gao HY, Yao WA, Yang ST. Study on steady-state thermal conduction with singularities in multi-material composites. International Journal of Heat and Mass Transfer, 2017, 104: 861-870.
[52]. Hu XF, Bui TQ, Wang JN, Yao WA, Tong LHT, Singh IV, Tanaka S. A new cohesive crack tip symplectic analytical singular element involving plastic zone length for fatigue crack growth prediction under variable amplitude cyclic loading. European Journal of Mechanics-A/Solids, 2017, 65: 79-90.
[53]. Hu XF, Gao HY, Yao WA, Yang ST. A symplectic analytical singular element for steady-state thermal conduction with singularities in composite structures. Numerical Heat Transfer, Part B: Fundamentals, 2016, 70: 406-419.
[54]. Zhou R, Zhu P, Li Z. The shielding effect of the plastic zone at mode-II crack tip. International Journal of Fracture, 2011, 171: 195-200.

Captions of figures and tables

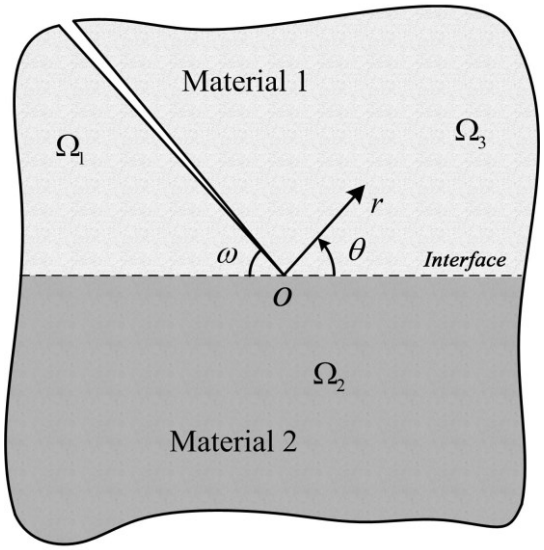

Fig.1 The configuration of inclined crack terminated at bimaterial interface

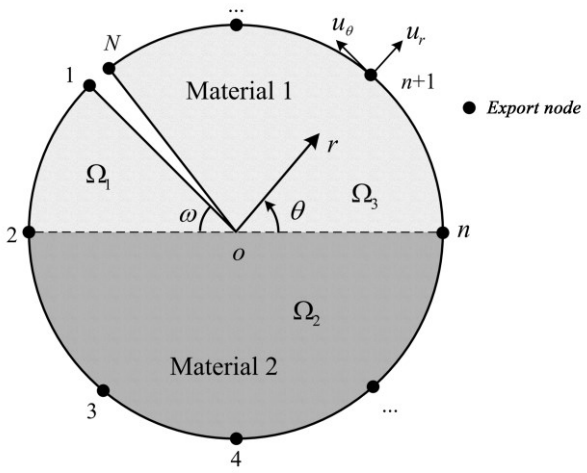

Fig.2 The configuration of the Symplectic Analytical Singular Element (SASE)

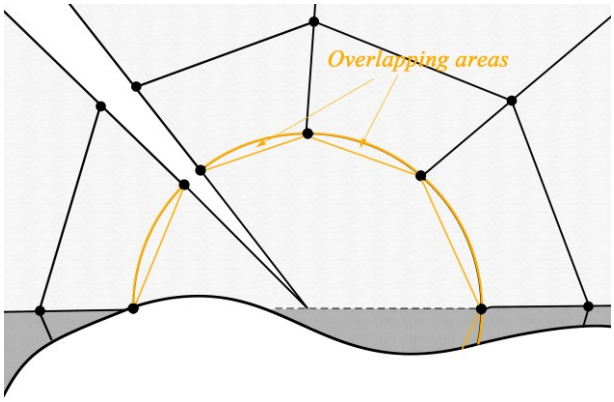

Fig.3 The overlapping areas between the SASE and conventional elements

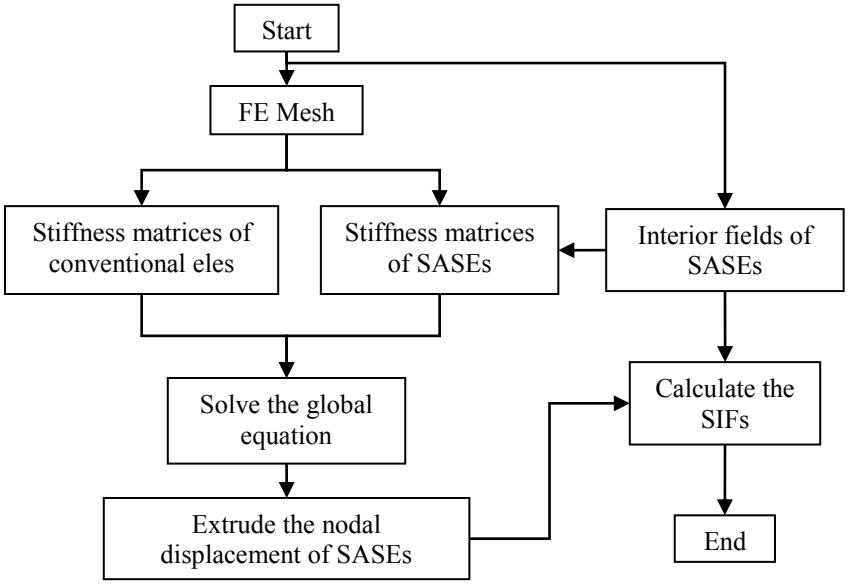

Fig.4 The solving procedure of the SASE

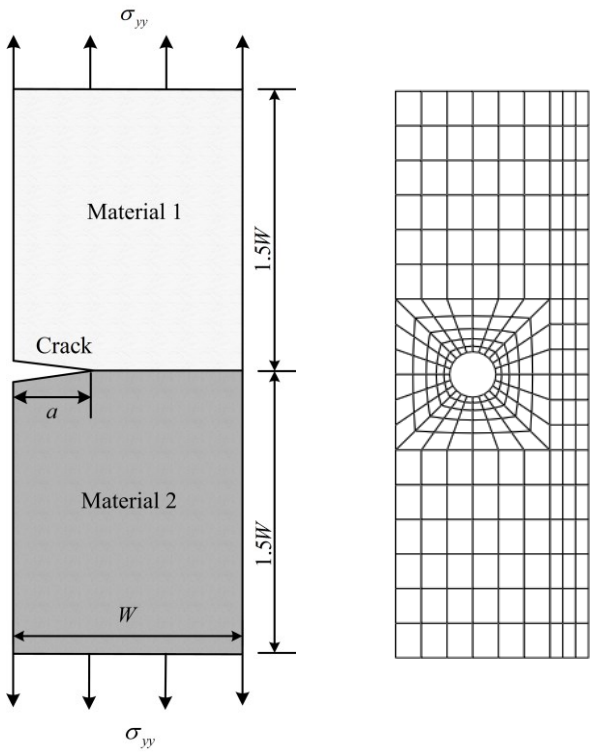

Fig.5 The configuration of an edge cracked bimaterial plate and the FE mesh

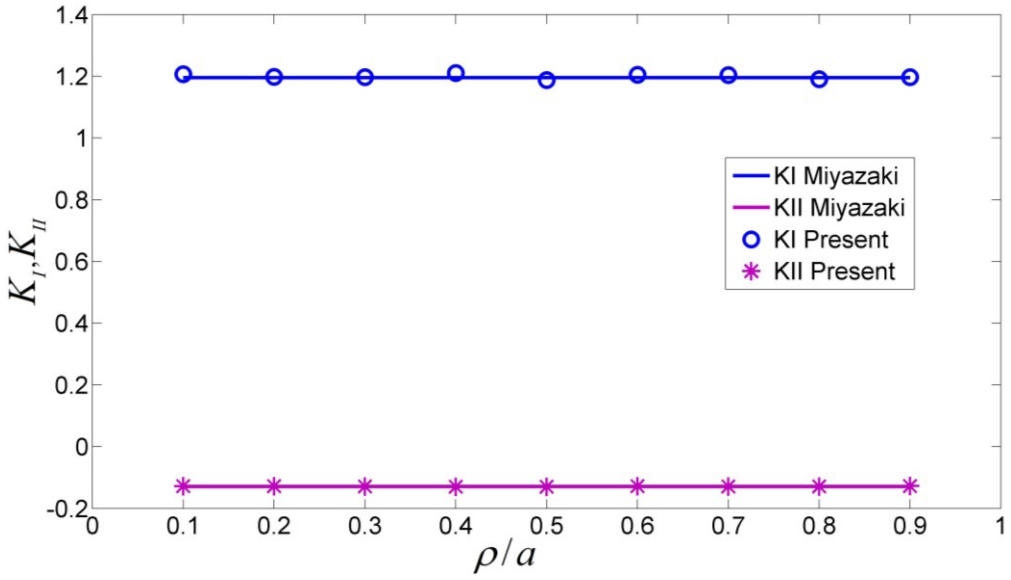

Fig.6 Variations of the predicted SIFs with the size of the SASE

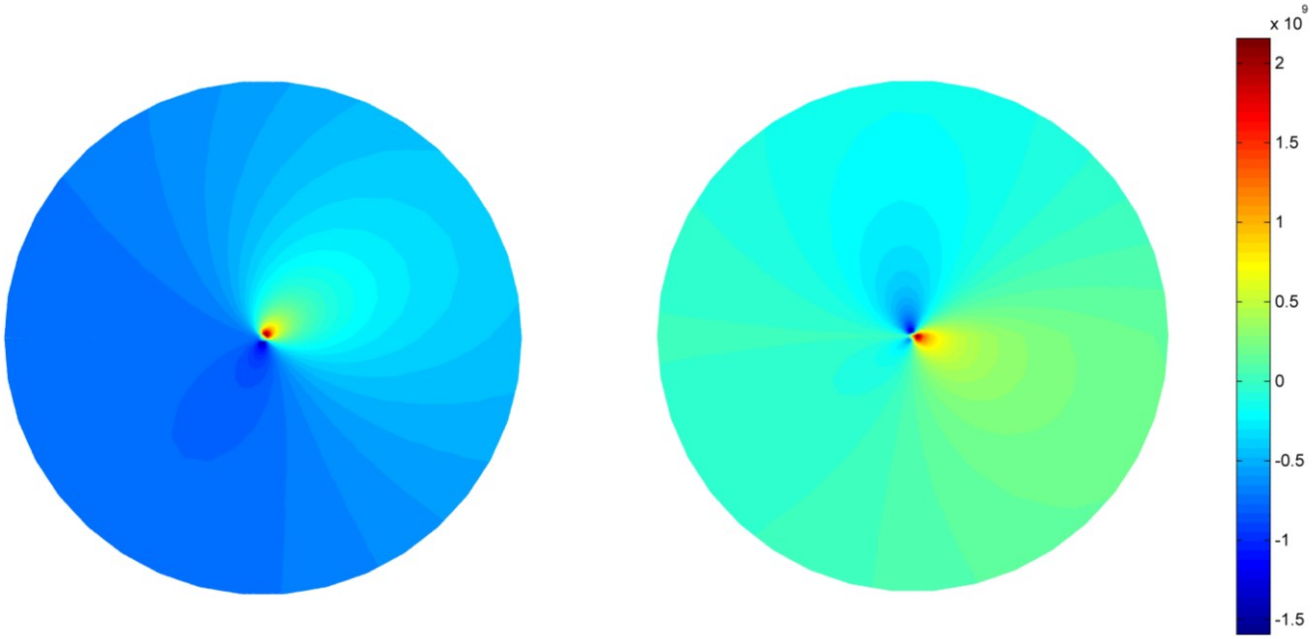

(a) σ_θ (b) $\sigma_{r\theta}$

Fig.7 Contours of the stress components in the vicinity of a bimaterial interface crack tip

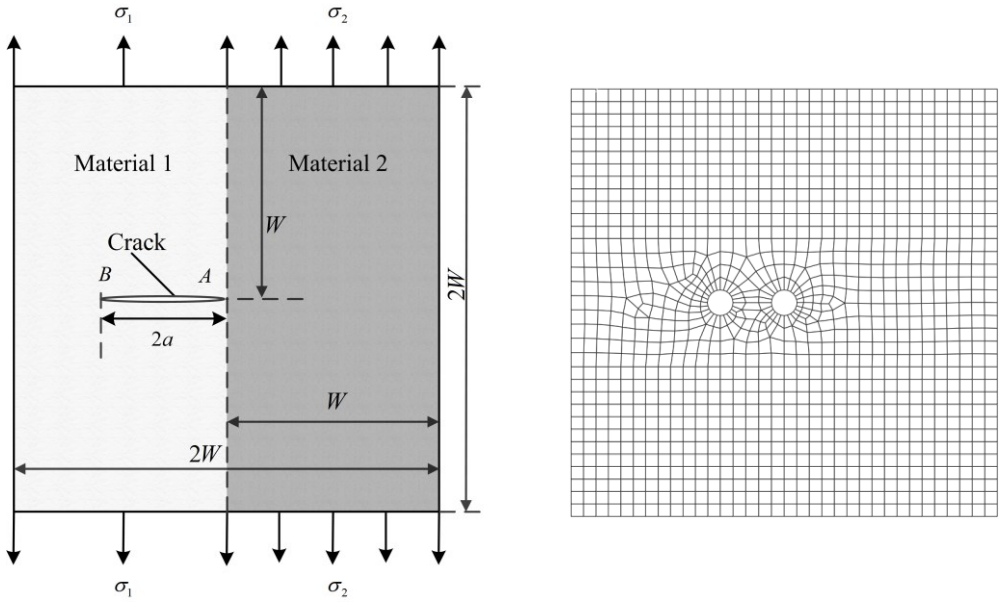

Fig.8 The configuration of a bimaterial plate containing an interior crack normal to the interface and the FE mesh

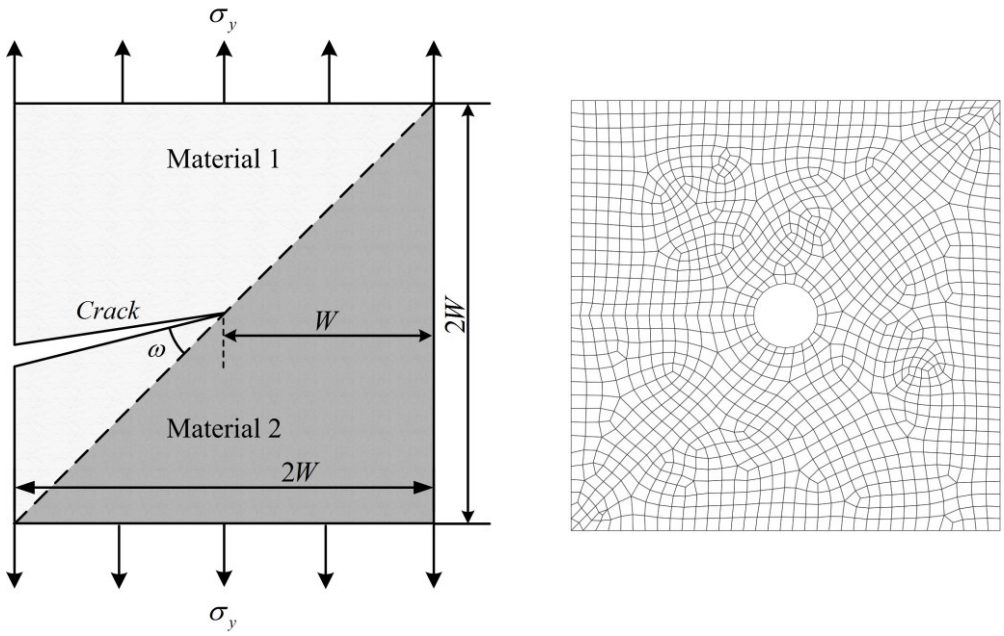

Fig.9 The configuration of a bimaterial plate containing an interior crack terminating at the interface and the FE mesh

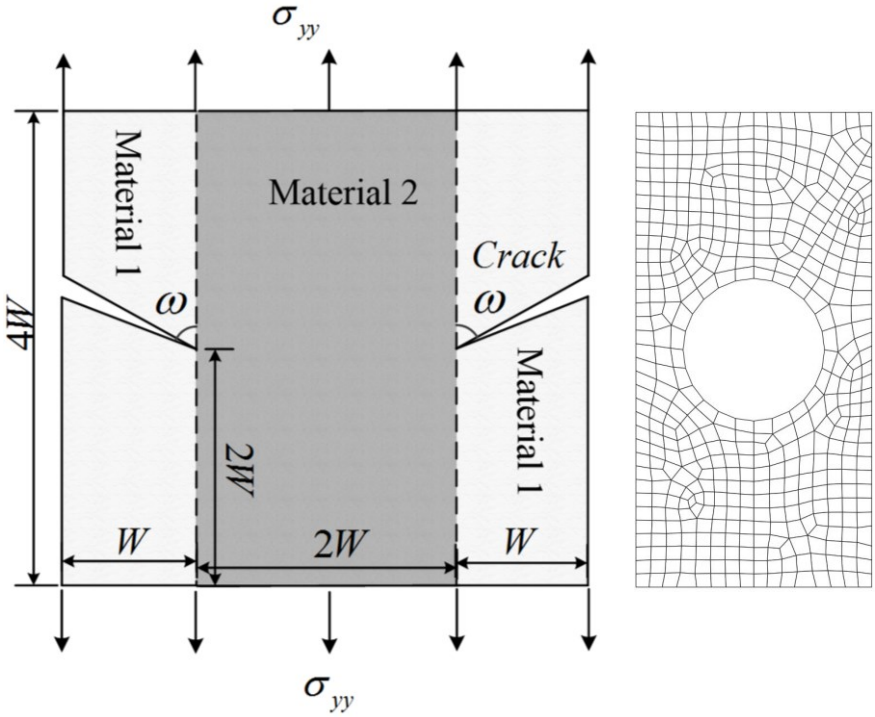

Fig.10 The configuration of a double edge cracked bimaterial plate and the FE mesh

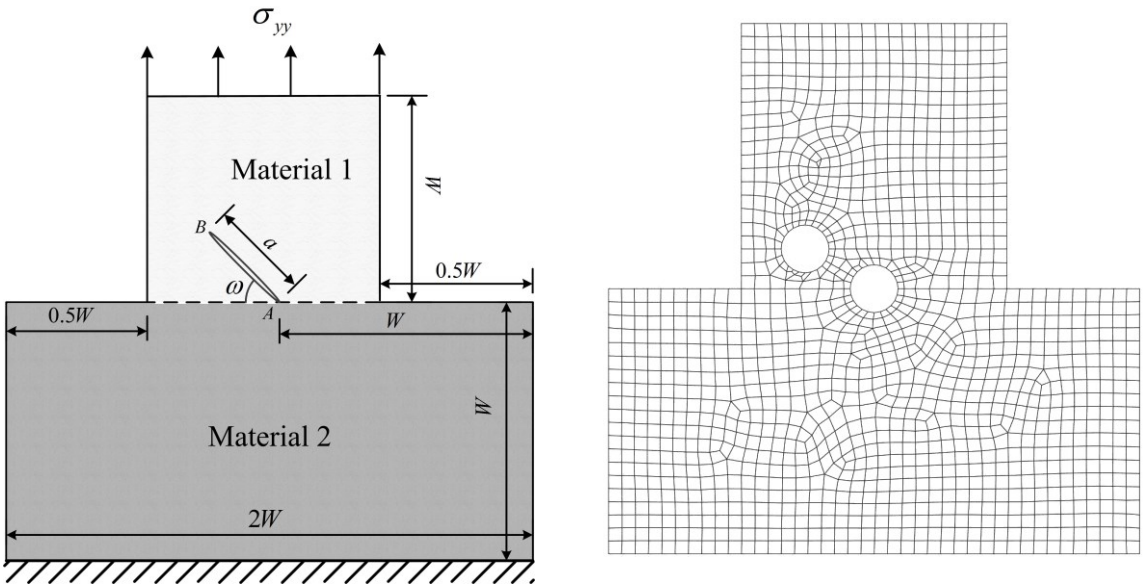

Fig.11 The configuration of a cracked bimaterial structure and the FE mesh

Tab.1 Numerical predictions of the non-dimensional SIFs for the cracked bimaterial plate

η	a/W	$K_{\mathrm{I}}/\sigma_{yy}\sqrt{\pi a}$		$K_{\mathrm{II}}/\sigma_{yy}\sqrt{\pi a}$	
		Present	Miyazaki[1]	Present	Miyazaki [1]
2	0.1	1.190	1.195	-0.130	-0.129
	0.2	1.364	1.367	-0.137	-0.137
	0.3	1.652	1.659	-0.158	-0.158
	0.4	2.101	2.110	-0.197	-0.198
3	0.1	1.198	1.203	-0.198	-0.197
	0.2	1.364	1.368	-0.207	-0.207
	0.3	1.650	1.656	-0.238	-0.239
	0.4	2.097	2.105	-0.297	-0.298
4	0.1	1.204	1.209	-0.241	-0.239
	0.2	1.365	1.368	-0.251	-0.250
	0.3	1.648	1.654	-0.288	-0.288
	0.4	2.093	2.101	-0.358	-0.359
10	0.1	1.225	1.229	-0.342	-0.340
	0.2	1.366	1.369	-0.350	-0.349
	0.3	1.643	1.648	-0.398	-0.399
	0.4	2.083	2.090	-0.492	-0.494
100	0.1	1.247	1.251	-0.428	-0.424
	0.2	1.368	1.370	-0.430	-0.428
	0.3	1.638	1.642	-0.484	-0.485
	0.4	2.073	2.078	-0.595	-0.597

Tab.2 Numerical results of the non-dimensional SIFs of the crack tip A

G_2/G_1	ν_1	ν_2	μ_s	Present	Chen[12]	Lin *et al*.[11]	Wang[13]	Cook[10]
0.00722	0.30	0.35	0.0749	0.020	0.019	0.020	0.019	0.079
0.0433	0.30	0.35	0.1758	0.096	0.095	0.095	0.096	0.074
0.5	0.30	0.30	0.4242	0.607	0.607	---	---	---
2.0	0.30	0.30	0.5721	1.629	1.626	---	---	---
23.08	0.35	0.30	0.7110	4.234	4.231	4.241	4.232	4.176
138.46	0.35	0.30	0.7335	5.001	5.001	4.978	5.002	4.922

Tab.3 Numerical results of the non-dimensional SIFs of the crack tip B

G_2/G_1	ν_1	ν_2	Present	Chen[12]	Lin et al.[11]	Wang[13]	Cook[10]
0.00722	0.30	0.35	1.500	1.474	1.529	1.474	1.509
0.0433	0.30	0.35	1.345	1.340	1.371	1.340	1.340
0.5	0.30	0.30	1.063	1.065	---	---	---
2.0	0.30	0.30	0.953	0.950	---	---	---
23.08	0.35	0.30	0.888	0.879	0.855	0.879	0.879
138.46	0.35	0.30	0.879	0.870	0.833	0.870	0.871

Tab.4 Numerical results of the non-dimensional SIFs of the inclined bimaterial interface crack

	$\omega=15^\circ$	$\omega=30^\circ$	$\omega=45^\circ$	$\omega=45^\circ$ [17]
μ_s	0.5303 ± 0.0746i	0.5648 ± 0.0667i	0.5996 ± 0.0448i	0.5996 ± 0.0448i
K_{I}	6.3740	7.5944	8.9794	8.9890
K_{II}	2.7036	2.6679	2.2099	2.0978

Tab.5 Numerical results of the non-dimensional SIFs of the crack orientation $\omega=90^\circ$

η	ν_1	ν_2	μ_s	Present K_I	ANSYS K_I
1.0	0.2	0.2	0.5	4.206	4.2196
1.0	0.2	0.3	0.5137	4.2484	---
2.0	0.2	0.3	0.5895	3.8396	---
4.0	0.2	0.3	0.6556	3.3399	---
8.0	0.2	0.3	0.7059	2.8437	---
16.0	0.2	0.3	0.7391	2.436	---
32.0	0.2	0.3	0.7588	2.1516	---

Tab.6 Numerical results of the non-dimensional SIFs of the crack orientation $\omega = 45^{o}$

η	ν_1	ν_2	μ_s	Present K_I	ANSYS K_I	Present K_{II}	ANSYS K_{II}
1.0	0.2	0.2	0.5	3.2385	3.2453	1.5029	1.5087
1.0	0.2	0.3	0.5077 ± 0.0133i	3.1412	---	1.5612	---
2.0	0.2	0.3	0.5706 ± 0.0235i	2.6047	---	1.6874	---
4.0	0.2	0.3	0.6213 ± 0.0395i	2.1643	---	1.5861	---
8.0	0.2	0.3	0.6549 ± 0.0622i	1.7944	---	1.3381	---
16.0	0.2	0.3	0.6739 ± 0.0800i	1.529	---	1.0977	---
32.0	0.2	0.3	0.6839 ± 0.0912i	1.3689	---	0.9361	---

Tab.7 Numerical results of the non-dimensional SIFs of the crack orientation $\omega = 30^{o}$

η	ν_1	ν_2	μ_s	Present K_I	ANSYS K_I	Present K_{II}	ANSYS K_{II}
1.0	0.2	0.2	0.5	2.6233	2.6272	1.6763	1.6866
1.0	0.2	0.3	0.5048 ± 0.0155i	2.4783	---	1.7335	---
2.0	0.2	0.3	0.5482 ± 0.0428i	1.9100	---	1.6305	---
4.0	0.2	0.3	0.5768 ± 0.0725i	1.4762	---	1.3513	---
8.0	0.2	0.3	0.5928 ± 0.0970i	1.1923	---	1.0696	---
16.0	0.2	0.3	0.6010 ± 0.1129i	1.0260	---	0.8743	---
32.0	0.2	0.3	0.6052 ± 0.1220i	0.9352	---	0.7603	---

Tab.8 Numerical results of the SIFs of crack tip A for different crack orientations

η	μ_s (90^o)	K_I (90^o)	μ_s (45^o)	K_I (45^o)	K_{II} (45^o)	μ_s (30^o)	K_I (30^o)	K_{II} (30^o)
10.0	0.7244	0.8232	0.6605 ± 0.0801i	1.4036	0.0896	0.5952-+0.1085i	1.4458	0.2393
100.0	0.7969	1.2741	0.6887 ± 0.1234i	1.7166	0.4156	0.6073-+0.1419i	1.5893	0.4258
1000.0	0.8062	1.4488	0.6915 ± 0.1287i	1.7493	0.4512	0.6085-+0.1457i	1.6048	0.4457

Tab.9 Numerical results of the SIFs of crack tip B for different crack orientations

η	K_I (90^o)	K_I (45^o)	K_{II} (45^o)	K_I (30^o)	K_{II} (30^o)
10.0	0.1051	0.6880	-0.4560	0.9357	-0.2991
100.0	0.0923	0.6678	-0.4525	0.9135	-0.2927
1000.0	0.0865	0.6655	-0.4520	0.9110	-0.2920